

CHEM MED CHEM

CHEMISTRY ENABLING DRUG DISCOVERY

Accepted Article

Title: Combined Scaffold Evaluation and Systems-level Transcriptome-Based Analysis for Accelerated Lead Optimization Reveals Ribosomal Targeting Spirooxindole Cyclopropanes

Authors: Kevin Rodriguez, Erin Howe, Emily Bacher, Miranda Burnette, Jennifer Meloche, Jayda Meisel, Patricia Schnepf, Xuejuan Tan, Mayland Chang, Jeremiah Zartman, Siyuan Zhang, and Brandon Lee Ashfeld

This manuscript has been accepted after peer review and appears as an Accepted Article online prior to editing, proofing, and formal publication of the final Version of Record (VoR). This work is currently citable by using the Digital Object Identifier (DOI) given below. The VoR will be published online in Early View as soon as possible and may be different to this Accepted Article as a result of editing. Readers should obtain the VoR from the journal website shown below when it is published to ensure accuracy of information. The authors are responsible for the content of this Accepted Article.

To be cited as: *ChemMedChem* 10.1002/cmdc.201900266

Link to VoR: <http://dx.doi.org/10.1002/cmdc.201900266>

WILEY-VCH

www.chemmedchem.org

A Journal of



FULL PAPER

Combined Scaffold Evaluation and Systems-level Transcriptome-Based Analysis for Accelerated Lead Optimization Reveals Ribosomal Targeting Spirooxindole Cyclopropanes

Kevin X. Rodriguez,^{[a]†} Erin N. Howe,^{[b]†} Emily P. Bacher,^[a] Miranda Burnette,^[c] Jennifer L. Meloche,^[a] Jayda Meisel,^[a] Patricia Schnepf,^[b] Xuejuan Tan,^[b] Mayland Chang,^[a] Jeremiah Zartman,^{[c]*} Siyuan Zhang^{[b]*} and Brandon L. Ashfeld^{[a]*}

- [a] K. X. Rodriguez, E. P. Bacher, J. L. Meloche, J. Meisel, Prof. Dr. M. Chang, Prof. Dr. B. L. Ashfeld
Department of Chemistry and Biochemistry
University of Notre Dame
305 McCourtney Hall, Notre Dame, IN 46556 (USA)
E-mail: bashfeld@nd.edu
- [b] E. N. Howe, P. Schnepf, X. Tan, Prof. Dr. S. Zhang
Department of Biological Sciences
University of Notre Dame
100 Galvin Life Science Center, Notre Dame, IN 46556 (USA)
Email: szhang8@nd.edu
- [c] M. Burnette, Prof. Dr. J. Zartman
Department of Chemical and Biological Engineering
University of Notre Dame
182 Fitzpatrick Hall, Notre Dame, IN 46556 (USA)
Email: jzartman@nd.edu

†These authors contributed equally to this work.

Supporting information for this article is given via a link at the end of the document.

Abstract: With evolutionary drug resistance impacting efforts to treat disease, the need for small molecules that exhibit novel molecular mechanisms of action is paramount. In this study, we have combined scaffold-directed synthesis with a hybrid experimental and transcriptome analysis to identify bis-spirooxindole cyclopropanes that inhibit cancer cell proliferation through disruption of ribosomal function. These findings demonstrate the value of an integrated, biologically-inspired synthesis and assay strategy for the accelerated identification of first-in-class cancer therapeutic candidates.

Introduction

Although target-based drug discovery is the most widely employed pharmacological strategy today,¹ recent retrospective analyses have revealed that more first-in-class small molecule leads are discovered through phenotypic screening.^{1b,2} However, a major challenge with this strategy is the lack of novel chemical space, which ultimately is of greater importance than the size of the library.³ Compared to *in silico* drug design, privileged core scaffolds of evolutionarily conserved active natural products⁴ can serve as a guide in diverting total synthesis to create structurally related small molecule libraries for functionally targeted phenotypic screens.^{4a,5} Therefore, phenotypic drug discovery based on pharmacologically active natural products remains a powerful strategy for rapidly evaluating the relevant chemical landscape in search of novel therapeutic mechanisms of action.⁶ However, lead identification and guided chemical optimization based on a defined molecular mechanism of action remains a time-consuming process. Herein, we present an integrative approach toward the synthesis and mechanism of action

identification of bis-spirooxindole cyclopropanes, inspired by 2-oxindole alkaloid natural products.

Oxindole alkaloids are a ubiquitous class of plant metabolites that exhibit a diverse array of potential therapeutic applications, including anti-mitotic activity in a number of cancer models.⁷ Of these, the C3-spirooxindole has emerged as a promising scaffold for chemotherapeutic design.⁸ Whether naturally occurring or designed, carbo- and heterocyclic spirooxindoles exhibit anti-viral, anti-cancer, and anti-inflammatory properties (Figure 1). Owing to the functionally diverse periphery and stereochemical density, many groups have sought to establish efficient synthetic strategies for the rapid construction of structurally diverse spirooxindole compound collections.⁹

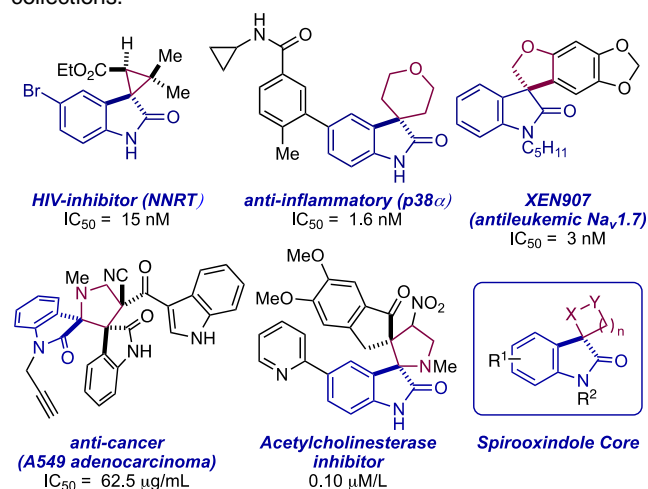


Figure 1. Biologically active spirooxindole small molecular targets.

FULL PAPER

Results and Discussion

Scaffold Validation

To evaluate the chemical space within 2-oxindoles, we synthesized an initial library of selected spirooxindoles bearing dihydrobenzofuranyl **1**, benzopyranyl **2**, and cyclopropyl rings **3** and **4** at the C3-spirocenter (Figure 2). Oxindoles **1-4** were screened for their anticancer activity using two isogenic human triple negative breast cancer cell lines, MDA-MB-231, and the brain metastatic derivative, MDA-MB-231-Br. Triple negative breast cancers are so named because they fail to express estrogen and progesterone receptors, and do not over-express Her2. Thus, these cancer cell lines were chosen as they often do not respond to hormone or anti-Her2 therapies, leaving chemotherapy as the only treatment option for patients suffering from this breast cancer subtype.

Representative dihydrobenzofuranyl and benzopyranyl spirooxindoles **1a** ($R^1 = R^3 = \text{Me}$, $R^2 = \text{H}$) and **2a** ($R^1 = R^3 = \text{Me}$, $R^2 = \text{H}$) showed low activity (63-87 μM) at inducing MDA-MB-231-Br cell death (Table 1). However, bisoxindole **2a** proved more effective against the less robust MDA-MB-231 cell line. Comparatively, cyclopropyl oxindoles **3a** ($R^1 = \text{Ts}$, $R^2 = \text{H}$, $R^3 = o\text{-BrC}_6\text{H}_4$, $R^4 = \text{Ph}$) and **4a** ($R^1 = \text{Ts}$, $R^2 = \text{H}$, $R^3 = o\text{-BrC}_6\text{H}_4$, $R^4 = \text{Ts}$, $R^5 = \text{H}$) were more active against MDA-MB-231-Br cells than either **1a** or **2a**, but showed poor activity against MDA-MB-231

Table 1. Representative lead spirooxindole activity.

Compound	R^1	R^2	R^3	R^4	R^5	EC_{50} (μM)	
						MDA-MB-231-Br	MDA-MB-231
1a	Me	H	Me	–	–	48.8	45.9
2a	Me	H	Me	–	–	54.0	8.2
3a	Ts	H	<i>o</i> -BrC ₆ H ₄	Ph	–	30.2	52.8
4a	Ts	H	<i>o</i> -BrC ₆ H ₄	Ts	–	30.1	66.8

comparable to **1a**. Given the more aggressive, metastatic nature of MDA-MB-231-Br cells, subsequent efforts focused on the spirocyclopropyl oxindole cores of **3a** and **4a**. Our second iteration (Figure 2a, below dashed line) revealed that compounds bearing the bis-spirooxindole cyclopropane **4** motif proved most efficacious against both the MDA-MB-231-Br and MDA-MB-231 cell lines. While less cytotoxic than most current anticancer therapeutics, this initial survey enabled lead identification of the bis-spirooxindole cyclopropane architectural core, and prompted further investigation of compounds derived from this subset.

Chemistry and Pharmacology

While synthetic efforts have focused on constructing C3-spiro-fused 5- and 6-membered rings,¹⁰ not until recently has the spirooxindole cyclopropane emerged as a scaffold for guided drug design.¹¹ In contrast to the rich history of 2-oxindoles, reports of spirooxindole cyclopropanes as architectural templates for therapeutic exploitation are limited.¹² Based on parallels drawn to known spirooxindole leads, as well as our initial compound screening, we targeted a series of derivatives around a central cyclopropane with (i) the 2-oxindole motif, (ii) an aromatic substituent, and (iii) geminal donor/acceptor functionality as three main points of variability (Figure 3).

To access the structural analogs of cyclopropyl oxindoles **4**, we sought a convergent fragment coupling synthetic strategy that enabled direct access to the core ring system while maintaining the flexibility required for architectural diversification. To accomplish this goal, we exploited a modification of the Kukhtin-Ramirez condensation reaction utilizing a phosphine-mediated cyclopropanation of β -aryl substituted alkylidene oxindoles with

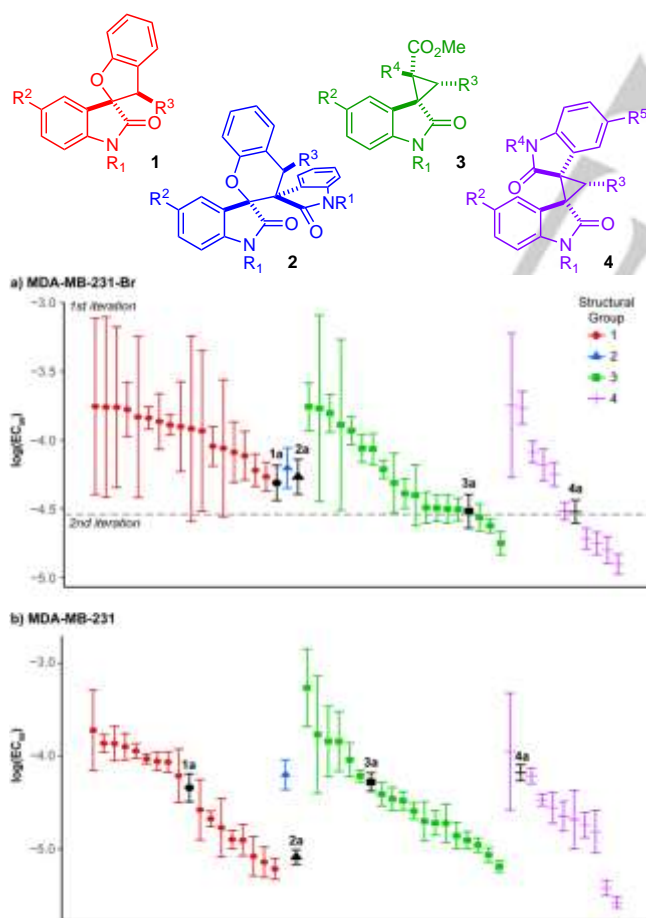


Figure 2. Oxindole framework with various spirofused rings being investigated. Identification of lead bis-spirooxindole framework **4** and $\log(\text{EC}_{50})$ values observed when screened against MDA-MB-231-Br human breast cancer cells.

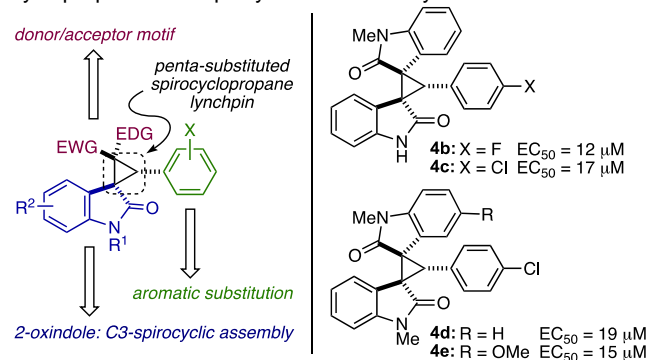
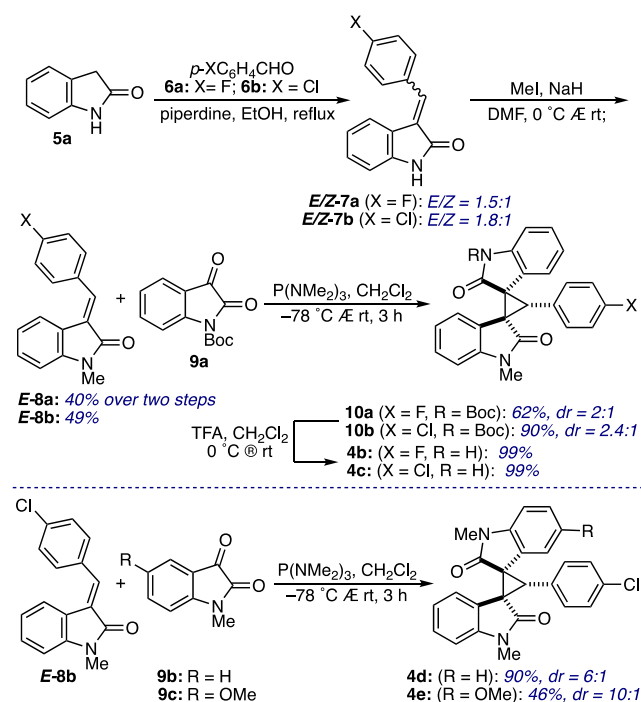


Figure 3. General molecular framework of the 3-spirocyclopropyl-2-oxindole core architecture with highlighted points of structural diversity. Primary lead compounds and EC_{50} values observed when screened for cytotoxicity against the human breast cancer (brain-seeking) MDA-MB-231-Br cell line.

FULL PAPER



Scheme 1. Syntheses of bispirooxindole cyclopropanes.

isatin derivatives.¹³ Employing this strategy, we synthesized bisoxindoles **4b** and **4c** in four steps beginning with the condensation of 2-oxindole (**5a**) and aryl aldehydes **6a** (X = F) and **6b** (X = Cl) to yield a mixture of alkylidenes **7a** (E/Z = 1.5:1) and **7b** (E/Z = 1.8:1) respectively (Scheme 1). The resulting E/Z mixtures were N-alkylated, and the alkylidene isomers separated to provide the desired E-alkylidene oxindoles **8a** (X = F) and **8b** (X = Cl). Separate treatment with N-Boc isatin (**9**) and P(NMe₂)₃ afforded bis-spirooxindole cyclopropanes **10a** and **10b** in 62% and 90% yield respectively as separable mixtures of only two diastereomers. Removal of the Boc group proceeded in quantitative yield to provide racemic **4b** and **4c**. The bis-N-methyl spirooxindole cyclopropanes **4b** and **4e** were synthesized following a similar three step sequence starting from either 2-oxindole (**5a**) or 5-methoxy-2-oxindole (**5b**) and employing N-methyl isatin in the P(NMe₂)₃-mediated cyclopropanation. This design strategy enabled us to assemble a collection of ~80 2-oxindole derivatives with site specific point substitutions on the benzenoid ring of the oxindole, donor/acceptor functional group variability, and substitution around the remaining aryl ring. Of these derivatives, compounds **4b-e** were identified as optimized hits in subsequent biological screenings.

Compounds **4b-e** have drug-like properties, as assessed by Lipinsky's rule of five (molecular weight <500, ClogP <5, hydrogen-bond donors <5, hydrogen-bond acceptors <10).¹⁴ Substitution of fluorine (**4b**) for chlorine (**4c**) lowered ClogP and increased the water solubility almost two-fold, and improved the potency against metastatic breast cancer cells (MDA-MB-231-Br) (Table 2).¹⁵ To evaluate blood-brain barrier permeability of oxindoles analogs, we calculated the topological polar surface area (tPSA). A tPSA range between 40-49 Å² indicates that the compounds may penetrate the blood-brain barrier.¹⁶ The average tPSA for the top 25 central nervous system drugs is 47 Å².¹⁷

Additionally, **4b-e** are stable in mouse plasma and rat liver S9 fractions, indicating that the compounds are metabolically stable.

RNA Sequencing and Molecular Mechanism of Action Prediction

The characterization of the molecular mechanism of action for novel compounds is a critical step in the drug discovery process. The development of high-throughput genomic analyses, combined with recently developed bioinformatic methods, can be harnessed to yield insight into the putative mechanism of action of a compound,^{1a} as well as a global assessment of off-target effects.^{2a,3b} To establish a mechanism of action-guided framework for chemical optimization, we selected oxindole **4b** for mechanism of action analysis (Figure 4). To identify time-dependent transcriptome shifting induced by **4b**, we treated MDA-MB-231-Br cancer cells with vehicle control (DMSO) or **4b** and performed RNA-sequencing. Given that prolonged treatment with **4b** induces apoptosis, we performed sequencing at 6, 12, and 24 hrs of treatment with **4b** (Figure 4A). These early timepoints provide insight into the transcriptome changes that occur in cells prior to activation of apoptotic pathways. Early transcriptome changes will be driven by the specific mechanism of action of the compound, allowing bioinformatic analysis to provide insight into the mechanism of action of **4b**.

The identification of robust transcriptome level changes in the majority of cells at early stages of treatment was ensured by conducting compound exposure at five times the EC₅₀ value reported at 5 days post-treatment (Table 2; 62 μM). After 24 h post-exposure, we identified 802 genes that were significantly down-regulated, while 928 genes were significantly up-regulated (p < 0.05). Expression of the top 400 differentially regulated genes shows a time-dependent progressive change from vehicle to 24 h treatment with **4b**, with some gene clusters being progressively down-regulated (Figure 4B, green) and others progressively up-regulated (Figure 4B, pink). This suggests that treatment with **4b** induces a time-dependent transcriptome shift over the course of 24 hours.

Bioinformatic analysis of the transcriptome provides an unbiased view of how cells respond to drug treatment, which potentially infers the mechanism of action of a drug candidate.^{4b,5f,6} Most small molecule therapeutics target proteins directly, as opposed to moderating protein activity at the transcriptional, or mRNA level. However, recent advances in gene network analysis have demonstrated the predictive power of transcriptome readouts for identifying the mechanism of action of a compound. One such approach – detecting mechanism of action by network dysregulation (DeMAND) analysis - predicts

Table 2. Representative lead spirooxindole activity

	4b	4c	4d	4e
clogP	2.91	3.48	3.86	3.78
tPSA	49.4	49.4	40.6	49.8
MW (g/mol)	384	401	415	445
Plasma stability t _{1/2} (h)	>2	>2	>2	>2
Rat S9 t _{1/2} (h)	>1	>1	>1	>1
EC ₅₀ MDA-231-Br (μM)	12	17	19	15
EC ₅₀ MDA-231 (μM)	22	3	2	18

FULL PAPER

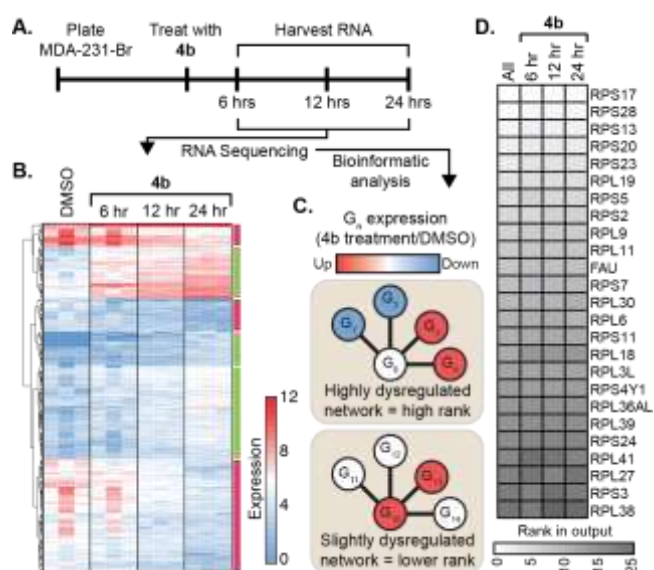


Figure 4. RNA-sequencing and mechanism of action Prediction. **A.** Schematic of experimental set-up. **B.** Heatmap depicting top 400 differentially up- (red) or down- (blue) regulated genes between DMSO and **4b** treatment conditions in MDA-MB-231-Br cells. Gene clusters are annotated as being progressively up-regulated (green), or progressively down-regulated (pink). **C.** Schematic of bioinformatic analysis method – detecting mechanism of action by network dysregulation (DeMAND). **D.** Top 25 ranked genes in the DeMAND output for each paired comparison. All: DMSO vs all **4b** treatment groups averaged; 6 h, 12 h, 24 h: paired comparison between each individual time point and DMSO.

the mechanism of action by examining differential expression of gene networks upon drug treatment, with the underlying assumption that although a drug's target protein may not be changed at the transcriptional level, the network of interacting proteins will be sufficiently dysregulated as to allow identification.¹⁸ First, DeMAND defines the regulon of each gene as a network of established interactions based on prior biological knowledge, such as the STRING network (Figure 4C, each brown square represent a single gene-level regulon).¹⁹ Next, DeMAND maps the observed transcriptome changes from RNA-sequencing analysis to the regulon of each gene (Figure 4C, G_n expression represented by red/blue colorbar). DeMAND then uses the dysregulation of regulons, rather than individual genes, to identify putative cellular targets (effectors). In the example in Figure 4C, although G_{10} is up-regulated with treatment, the entire regulon is relatively unaffected, while G_0 has a strongly dysregulated regulon. Here, G_0 would be ranked more highly as being involved in the mechanism of action due to the dysregulation of effectors.

In an effort to predict the mechanism of action of the spirocyclopropyl oxindoles, we input the RNA-sequencing data obtained for **4b** into the DeMAND algorithm. The DeMAND analysis returns a ranked list of genes that corresponds to the probability that a particular gene is an effector, based on the dysregulation of that gene's network. As **4b** is a novel compound, we had no knowledge *a priori* regarding the speed with which **4b** would induce transcriptional changes. Thus, analysis was conducted in two ways: 1) each individual **4b** treatment time point (e.g. 6 h) was compared to the DMSO control; 2) the average expression across all **4b** treatment timepoints was compared to the DMSO (labeled All in Figure 4D). Depicted based on rank, with rank 1 being most likely to be an effector, the top 25 effector genes

of **4b** predicted by DeMAND (Figure 4D) consistently identified the same set of effector genes across all time points. The top 25 ranked effectors within the dysregulated regulons were evident as early as 6 h and persisted through 24 h post treatment (Figure 4B), suggesting a **4b**-specific mechanism of action.

DeMAND identified 9831 genes as possible mechanism of action mediators with a false discovery rate (FDR) of < 0.05 , and 1732 genes with FDR q -value $< 1E^{-5}$ (Table S7). To explore common functionality of mechanism of action mediators, we performed Gene Set Enrichment Analysis (GSEA).²⁰ GSEA utilizes lists of genes (gene sets), which are grouped by biological activity, including common function, sequence homology, or chromosomal location. Each gene set is compared to a ranked input file, to determine the rank of each gene in the gene set. If the input genes fall near the top of the list, the gene set is positively enriched, if they fall near the bottom of the list, the gene set is negatively enriched. For our data, genes were ranked by their DeMAND predicted significance (inverse p -value) and assigned directionality by their differential expression. GSEA analysis identified 125 positively enriched gene sets (induced by **4b** treatment, Table S8) and 231 negatively enriched gene sets (inhibited by **4b** treatment, Table S9) with FDR q -value $< 1E^{-3}$.

Interestingly, the KEGG Ribosome pathway had the highest negative enrichment score, -9.45 (Figure 5A), suggesting that this gene set is significantly negatively regulated by **4b** treatment. Several of the top 15 negatively enriched gene sets represent either the structural components of the ribosome (Figure 5A, dark green bars), the function of the ribosome (Figure 5A, medium green bars), or activities that are related to or dependent on ribosomal function (Figure 5A, light green bars). Indeed, the top 25 DeMAND predicted genes exclusively encode ribosomal proteins (Figure 4D), and 75% of the top 100 ranked genes encode ribosomal proteins.²¹

To further explore the specificity of the predicted mechanism of action of **4b**, we curated custom gene sets that represent distinct mechanism of action classes of various, well-characterized anti-cancer therapeutics, namely 1) apoptosis, 2) cell cycle regulation, 3) regulation of the ribosome, 4) disruption of microtubule function, 5) DNA damage, 6) kinase activation, 7) G-protein coupled receptor (GPCR) signaling, and 8) ion channel signaling.²² Given that the majority of cytotoxic agents exhibit a mechanism of action covered by one of these broad categories, we determined the enrichment of each of these gene sets in the DeMAND results. Analysis revealed that the top 100 predicted **4b** mechanism of action effector genes cluster strongly in the ribosome regulation class, without overlapping with other common drug mechanism of action gene sets (Figure 5B). This strongly suggests that **4b** cytotoxicity is due to inhibition of ribosomal function.

Next, we sought to validate the effect of **4b** on ribosomal function by evaluating its impact on protein translation. The breast cancer cell line MDA-MB-231-Br was treated separately with DMSO (vehicle), doxorubicin (DNA intercalating agent), paclitaxel (microtubule stabilizer), cyclohexamide (protein synthesis inhibitor), and compounds **4b** and **4c** for 4 h, then subjected to a fluorescence-based methionine incorporation assay to evaluate the impact of each on protein synthesis (Figure 5C). Those cells treated with **4b** exhibited a decrease in protein synthesis comparable to cells treated with the positive control cycloheximide, and a substantial decrease in comparison to the negative controls doxorubicin and paclitaxel (Figure 5C and 5D).

FULL PAPER

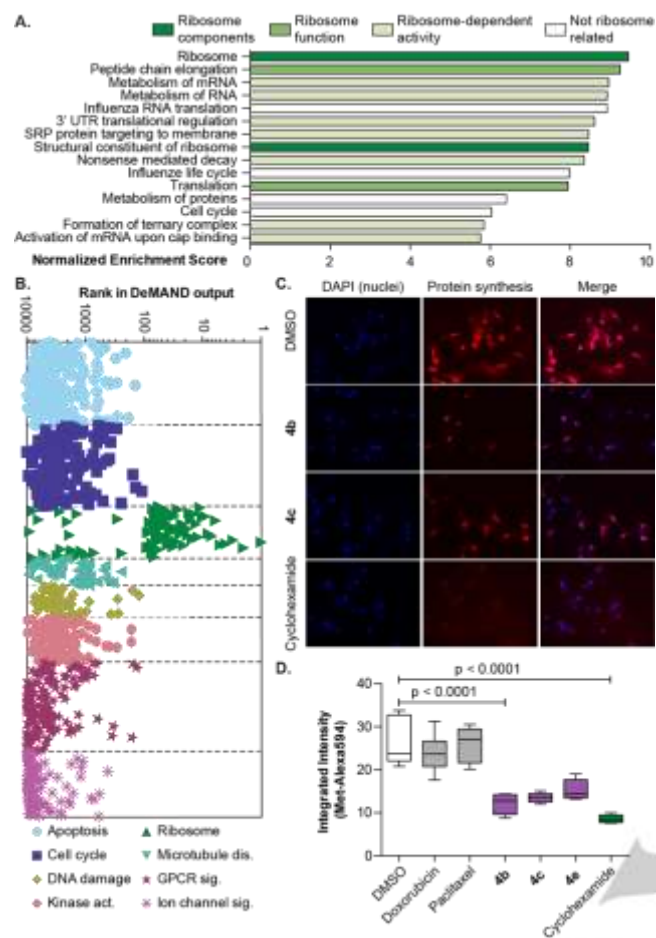


Figure 5. Inhibition of ribosomal function and translation by **4b**. **A.** The rank of DeMAND predicted effectors of **4b** treatment in MDA-231-Br cells was used as input for gene set enrichment analysis (GSEA). Top fifteen gene sets predicted by GSEA to be negatively enriched following **4b** treatment. Dark green bars, gene sets representing components of the ribosome. Medium green bars, gene sets representing the function of the ribosome. Light green bars, gene sets representing cellular processes related to translation. White bars, gene sets not related to ribosomal structure or function. **B.** Gene sets were compiled to represent the common drug MoA of current cancer treatment options, and each MoA is assigned a color and symbol as shown top. For all genes represented by these 8 common MoA classes that were in the top 10,000 DeMAND predicted effectors of **4b** MoA, the DeMAND rank is shown. **C.** MDA-MB-231-Br cells were treated for four hours and subjected to a fluorescent methionine incorporation assay. Representative images are shown. Red: methionine incorporation for protein synthesis. Blue: DAPI staining for nuclei. **D.** Quantitation of data shown in C, methionine signal is normalized to number of cells per field as indicated by DAPI staining. Boxes, first to third quartile range of 10 images per condition, line, mean, whiskers, full range of data points. One-way ANOVA with Dunnett's multiple comparison test.

The combination of advanced DeMAND transcriptome analysis and data obtained from the protein synthesis assay strongly suggests that spirocyclopropyl oxindole **4b** rapidly targets ribosome function, resulting in an mechanism of action that includes inhibition of mRNA protein translation, which negatively impacts the proliferation and subsequent survival of rapidly dividing cancer cells.

Conclusions

In summary, by employing an integrated spirooxindole scaffold synthesis, phenotypic evaluation, and transcriptome analysis

approach toward drug design, we identified a series of bispirooxindole cyclopropanes that exhibit a ribosomal-targeting mechanism of action toward limiting cancer cell proliferation. These results suggest that our lead compounds exhibit an intriguing mechanism of action of targeting ribosomal processes. Since translation of mRNA into protein is an incredibly energy-consuming process, inhibition of translation is under investigation as a promising cancer therapeutic strategy.²³ Historically, defining the structure and function relationship of pharmacologically active natural products has been a largely empirical process that lacks molecular level insight. Biologically inspired total synthesis, coupled with global bioinformatics analysis of transcriptome networks, constitutes an alternative strategy for the rapid identification of potent bioactive lead candidates with clear molecular level details of mechanism of action. Our study illustrates how an accelerated phenotypic drug discovery process incorporating elements of target-directed scaffold assembly and transcriptome bioinformatics analysis can lead to the identification and biomolecular characterization of therapeutic lead compounds.

Experimental Section

General. Solvents and reagents were ACS reagent grade and used without further purification unless noted below. Dimethylformamide (DMF), tetrahydrofuran (THF), dichloromethane (CH_2Cl_2) and diethyl ether (Et_2O) were passed through a column of molecular sieves and stored under argon. All reactions were carried out in flame-dried glassware under an argon atmosphere unless otherwise specified. Spirocyclopropyl oxindoles **3a**, **4a**, alkylidene oxindoles **8**^{13a,24} and isatin derivatives **9**^{24b,25} were prepared according to literature procedures and spectral data (^1H NMR and ^{13}C NMR) were consistent with reported data. The relative stereochemistry of **4d** was unambiguously assigned using X-ray crystallography, and the relative stereochemistry for **10a**, **10b**, **4b-4e** were assigned by comparison of ^1H NMR and ^{13}C NMR data.

^1H Nuclear magnetic resonance (NMR) spectra were obtained at 600 MHz, and ^{13}C NMR spectra at 100, 125 or 150 MHz. Chemical shifts are reported in parts per million (ppm, δ), and referenced to residual solvent or tetramethylsilane (TMS). Coupling constants are reported in Hertz (Hz). Spectral splitting patterns are designated as s, singlet; d, doublet; t, triplet; q, quartet; p, pentet; m, multiplet; comp, complex; app, apparent; hom, higher order multiplet; and br, broad. Infrared (IR) spectra were obtained using a Thermo Electron Nicolet 380 FT-IR using a silicon (Si) crystal in an attenuated total reflectance (ATR) tower and reported as wavenumbers (cm^{-1}). High and Low resolution electrospray ionization (ESI) measurements were made with a Bruker MicroTOF II mass spectrometer. Analytical thin layer chromatography (TLC) was performed using EMD 250 micron 60 F254 silica gel plates, visualized with UV light and stained with a p-anisaldehyde solution. Flash column chromatography was performed according to Still's procedure (Still, W. C.; Kahn, M.; Mitra, A. J. *Org. Chem.* 1978, 43, 2923) using EMD 40-63 μm 60Å silica gel.

General procedure for the synthesis of benzofuranylspirooxindoles. Methyl lithium (0.45 mmol, 0.28 mL, 1.6 M) was dropwise added to a solution of Boc-salicylaldehyde (66.7 mg, 0.30 mmol) in THF (3 mL) at -78°C . After 5 minutes, hexamethylphosphorotriamide (53.8 mg, 0.30 mmol) was slowly added after which a solution of *N*-isatin derivative (48.3 mg, 0.30 mmol) in 1 mL of THF was dropwise added to the reaction mixture. The mixture was allowed to warm slowly to rt over a period of 2-2.5 h by removal of the dry ice/acetone bath. The reaction was concentrated under reduced pressure and the crude material was run under a small plug of silica gel eluting with ethyl acetate and concentrated. The residue was

FULL PAPER

purified by flash chromatography eluting with hexanes/ethyl acetate (3:1) to provide 43.7 mg (55%) of **1a** in a 2:1 diastereometric ratio as a light red solid and 30.8 mg (25%) of **2a** as a red solid in a 4:1 diastereometric ratio. Diastereometric ratios were determined by ¹H NMR or HPLC analysis.

1',3'-Dimethyl-3H-spiro[benzofuran-2,3'-indolin]-2'-one (1a).

Diastereoselectivity was determined by analysis of the 500 MHz ¹H NMR spectra (**A**: 4.01 (q, 1 H); **B**: 3.92 (q, 1 H)). ¹H NMR (500 MHz, CDCl₃) **Diastereomer A**: δ 7.35 (t, *J* = 8 Hz, 1 H), 7.20-7.16 (comp, 2 H), 7.09 (d, *J* = INSERT Hz, 1 H), 7.00-6.96 (m, 2 H), 6.88-6.86 (comp, 2 H), 4.01 (q, *J* = 7.2 Hz, 1 H), 3.24 (s, 3 H), 1.13 (d, *J* = 7.2 Hz, 3 H), **Diastereomer B**: δ 7.35 (t, *J* = 8 Hz, 1 H), 7.20-7.16 (comp, 2 H), 7.09 (d, *J* = 8 Hz, 1 H), 7.00-6.96 (m, 2 H), 6.88-6.86 (comp, 2 H), 3.92 (q, *J* = 7.1 Hz, 1 H), 3.18 (s, 3 H), 1.34 (d, *J* = 7.1 Hz, 3 H); ¹³C NMR (125 MHz, CDCl₃) **Diastereomer A**: δ 175.75, 158.86, 143.89, 131.27, 130.65, 128.66, 125.39, 123.92, 122.97, 121.64, 110.13, 108.90, 90.15, 43.82, 26.74, 15.21, **Diastereomer B**: δ 175.75, 158.86, 143.89, 130.77, 128.76, 126.06, 124.34, 123.60, 123.53, 121.59, 110.13, 108.90, 90.15, 46.37, 27.90, 13.78; IR (neat) 2961, 2927, 2872, 2853, 1725, 1612, 1595, 1494, 1468, 1373, 1224, 1120, 970, 862 cm⁻¹; HRMS (ESI) *m/z* 266.1173 [C₁₇H₁₅NO₂ (M+H) requires 266.1176]; m.p. = 100-105 °C.

1,1',4'-Trimethyldispiro[indoline-3,2'-chromane-3',3''-indoline]-

2,2''-dione (2a). Diastereoselectivity was determined by analysis of the 500 MHz ¹H NMR spectra (**A**: 4.49 (q, 1 H); **B**: 4.00 (q, 1 H)). ¹H NMR (500 MHz, CDCl₃) **Diastereomer A**: δ 7.37-7.31 (m, 2 H), 7.24-7.18 (m, 2 H), 7.06-7.00 (m, 2 H), 6.94 (t, *J* = 8.1 Hz, 2 H), 6.74 (t, *J* = 8.1 Hz, 2 H), 6.57 (t, *J* = 7.6 Hz, 1 H), 5.78 (d, *J* = 7.6 Hz, 1 H), 4.49 (q, *J* = 6.9 Hz, 1 H), 3.20 (s, 3 H), 2.88 (s, 3 H), 0.92 (d, *J* = 6.9 Hz, 3 H), **Diastereomer B**: δ 7.39-7.28 (m, 4 H), 7.13 (t, *J* = 7.6 Hz, 1 H), 7.08-6.97 (m, 5 H), 6.87 (d, *J* = 7.8 Hz, 1 H), 6.83 (d, *J* = 7.8 Hz, 1 H), 4.00 (q, *J* = 6.5 Hz, 1 H), 3.14 (s, 3 H), 3.07 (s, 3 H), 0.92 (d, *J* = 6.5 Hz, 3 H), ¹³C NMR (125 MHz, CDCl₃) **Diastereomer A**: δ 174.85, 172.99, 152.56, 144.96, 144.57, 130.89, 129.03, 128.15, 127.28, 126.23, 126.06, 125.87, 124.90, 124.60, 123.07, 122.07, 122.02, 116.65, 108.33, 108.18, 78.94, 55.55, 30.68, 26.39, 26.30, 13.47, **Diastereomer B**: δ 173.82, 170.97, 152.77, 143.81, 143.64, 130.42, 128.74, 128.66, 127.75, 127.23, 126.32, 125.72, 125.53, 125.30, 123.12, 123.09, 122.65, 117.97, 108.31, 107.94, 80.75, 54.65, 33.21, 26.56, 26.54, 13.90; IR (neat) 2965, 1724, 1709, 1610, 1469 cm⁻¹; HRMS (ESI) *m/z* 411.1738 [C₂₆H₂₃N₂O₃ (M+H) requires 411.1703]; m.p. = >260 °C.

General procedure for the synthesis of bispiroindole cyclopropanes. A two-dram scintillation vial, equipped with a magnetic stir bar, was charged with alkylidene oxindole (**E**-**8** (1 equiv) and isatin **9** (1.5 equiv). Dry, degassed CH₂Cl₂ (0.25 M) was added, the resulting solution cooled to -78 °C and stirred for 5 min. Then P(NMe₂)₃ (1.5 equiv) was added dropwise, and the mixture allowed to warm slowly to rt over a period of 2-2.5 h by removal of the dry ice/acetone bath. The solution was immediately concentrated under reduced pressure, and the resulting crude mixture was purified by flash chromatography eluting with hexanes/EtOAc at the indicated ratio to provide the title bis-spiroindole cyclopropane **10**.

tert-Butyl-3'-(4-fluorophenyl)-1''-methyl-2,2''-dioxodispiro[indoline-3,1'-cyclopropane-2',3''-indoline]-1-carboxylate (10a).

Cyclopropanation of (**E**-**8a**)^{13a} (152 mg, 0.60 mmol) with **9a**^{25b} (178 mg, 0.72 mmol), purified by flash chromatography eluting with hexanes/EtOAc (4:1), provided 145 mg (50 %) in a 1:1 diastereometric ratio of **10a** as a light yellow solid. Diastereoselectivity was determined by ¹H NMR (500 MHz) analysis (**A**: 4.38 (s, 1 H); **B**: 4.40 (s, 1 H)). ¹H NMR (600 MHz, CDCl₃) δ 8.03 (d, *J* = 7.8, 1.2 Hz, 1 H), 7.76 (d, *J* = 8.4 Hz, 1 H), 7.33 (td, *J* = 7.8, 1.2 Hz, 1 H), 7.26 (td, *J* = 7.8, 1.2 Hz, 1 H), 7.23 (td, *J* = 7.8, 1.2 Hz, 1 H), 7.05-7.02 (comp, 2 H), 6.98-6.96 (comp, 2 H), 6.89 (td, *J* = 8.4, 1.2, Hz, 1 H), 6.84 (d, 7.2 Hz, 1 H), 4.38 (s, 1 H), 3.21 (s, 3 H), 1.54 (s, 9 H); ¹³C NMR (150 MHz, CDCl₃) δ 171.0, 167.1, 163.0, 161.4, 148.7, 144.3, 139.6, 132.0, 131.9, 128.8, 128.5, 128.3, 125.6, 124.8, 124.8, 123.4, 123.1, 121.6, 120.7, 115.1, 115.0, 114.0, 107.6, 84.4, 49.0, 46.2, 39.3, 28.1, 26.8; **Diastereomer B**: ¹H NMR (600 MHz, CDCl₃) δ 7.93

(d, *J* = 7.8 Hz, 1 H), 7.77 (d, *J* = 7.8 Hz, 1 H), 7.33 (td, *J* = 7.2, 1.2 Hz, 1 H), 7.26 (comp, 1 H), 7.12 (td, *J* = 7.2, 1.2 Hz, 1 H), 7.09 (dd, *J* = 7.8, 1.2 Hz, 1 H), 7.05-7.03 (m, 2 H), 7.00-6.95 (m, 3 H), 6.85 (d, *J* = 7.8 Hz, 1 H), 4.40 (s, 1 H), 3.14 (s, 3 H), 1.60 (s, 9 H); ¹³C NMR (150 MHz, CDCl₃) δ 169.8, 168.7, 163.1, 161.4, 148.7, 143.8, 140.1, 132.1, 132.1, 128.9, 128.4, 128.3, 125.7, 124.7, 124.7, 123.8, 122.8, 122.0, 120.2, 115.1, 115.0, 113.7, 107.6, 84.6, 48.3, 46.7, 39.5, 28.1, 26.5; IR (neat) 2989, 2933, 1763, 1726, 1712, 1609, 1513, 1466, 1353, 1294, 1251, 1148, 1089, 748 cm⁻¹; HRMS (ESI) *m/z* 507.1703 [C₂₉H₂₅FN₂O₄ (M+Na) requires 507.1691]; m.p. > 200 °C.

tert-Butyl-3'-(4-chlorophenyl)-1''-methyl-2,2''-dioxodispiro[indoline-3,1'-cyclopropane-2',3''-indoline]-1-carboxylate (10b).

Cyclopropanation of (**E**-**8b**)^{24b} (53.9 mg, 0.20 mmol) with **9a**^{25b} (48.3 mg, 0.30 mmol), purified by flash chromatography eluting with hexanes/EtOAc (4:1), provided 51 mg (51%) in a 2.3:1 diastereometric ratio of **10b** as a light yellow solid. Diastereoselectivity was determined by ¹H NMR (500 MHz) analysis (**A**: 4.34 (s, 1 H); **B**: 4.36 (s, 1 H)). Major diastereomer: ¹H NMR (500 MHz, CDCl₃) δ 8.03 (d, *J* = 7.8 Hz, 1 H), 7.67 (d, *J* = 8.2 Hz, 1 H), 7.35 (t, *J* = 7.8 Hz, 1 H), 7.29-7.22 (m, 4 H), 7.05 (d, *J* = 6.0 Hz, 1 H), 7.01 (d, *J* = 8.2 Hz, 2 H), 6.90 (t, *J* = 7.8 Hz, 1 H), 6.85 (d, *J* = 7.8 Hz, 1 H), 4.37 (s, 1 H), 3.22 (s, 3 H), 1.54 (s, 9 H); ¹³C NMR (125 MHz, CDCl₃) δ 171.1, 167.3, 148.9, 144.6, 139.9, 133.8, 131.9, 129.0, 128.8, 128.6, 128.5, 127.9, 125.8, 123.6, 123.3, 121.9, 120.9, 114.2, 107.8, 84.6, 49.1, 46.4, 39.5, 28.3, 27.0; IR (neat) 3018, 2980, 1787, 1761, 1716, 1611, 1493, 1466, 1350, 1151 cm⁻¹; HRMS (ESI) *m/z* 523.1384 [C₂₉H₂₅ClN₂O₄ (M+Na) requires 523.1395]; m.p. = 199 °C.

3'-(4-Chlorophenyl)-1,1''-dimethyldispiro[indoline-3,1'-

cyclopropane-2',3''-indoline]-2,2''-dione (4d). Cyclopropanation of (**E**-**8b**)^{24b} (37.6 mg, 0.14 mmol) with *N*-methylisatin^{25a} **9b** (32.2 mg, 0.20 mmol), purified by flash chromatography eluting with hexanes/EtOAc (3:1), provided 52 mg (90%) in a 6:1 diastereometric ratio of **4d** as a light yellow solid. Diastereoselectivity was determined by ¹H NMR (500 MHz) analysis (**A**: 4.36 (s, 1 H); **B**: 4.73 (s, 1 H)). Major diastereomer: ¹H NMR (500 MHz, CDCl₃) δ 8.06 (d, *J* = 10 Hz, 1 H), 7.34 (td, *J* = 1.0, 7.5 Hz, 1 H), 7.29-25 (m, 3 H), 7.18-7.13 (comp, 2 H), 7.02 (d, *J* = 10 Hz, 2 H), 6.91 (td, *J* = 1.0, 7.5 Hz, 1 H), 6.85 (dd, *J* = 7.5, 1.5 Hz, 2 H), 4.36 (s, 1 H), 3.23 (s, 3 H), 3.15 (s, 3 H); ¹³C NMR (125 MHz, CDCl₃) δ 172.0, 169.6, 144.5, 144.0, 133.7, 132.0, 129.3, 128.6, 128.5, 128.4, 128.4, 126.0, 124.7, 121.9, 121.5, 121.5, 107.7, 47.8, 45.7, 39.8, 27.0, 26.7; IR (neat) 2981, 2923 2855, 1764, 1710, 1708, 1609, 1467, 1343, 1088, 748 cm⁻¹; HRMS (ESI) *m/z* 437.1027 [C₂₅H₁₉ClN₂O₂ (M+Na) requires 437.1027]; m.p. = 100-105 °C.

3'-(4-Chlorophenyl)-5-methoxy-1,1''-dimethyldispiro[indoline-3,1'-cyclopropane-2',3''-indoline]-2,2''-dione (4e).

Cyclopropanation of (**E**-**8b**)^{24b} (37.6 mg, 0.14 mmol) with 5-methoxy-1-methylindoline-2,3-dione²⁶ **9c** (32.2 mg, 0.20 mmol), purified by flash chromatography eluting with hexanes/EtOAc (3:1), provided 30 mg (46%) in a 10:1 diastereometric ratio of **4e** as a green-gray solid. Diastereoselectivity was determined by ¹H NMR (400 MHz) analysis (**A**: 4.32 (s, 1H); **B**: 4.37 (s, 1H)). Major diastereomer: ¹H NMR (400 MHz, CDCl₃) δ 7.81 (d, *J* = 4.0 Hz, 1H), 7.31-7.27 (comp, 2H), 7.23 (dd, *J* = 0.8, 6.8 Hz, 1H), 7.06-7.04 (comp, 2H), 6.94 (td, *J* = 1.2, 8.0 Hz, 1H), 6.90 (d, *J* = 2.8 Hz, 1H), 6.88 (d, *J* = 2.4 Hz, 1H), 6.86 (d, *J* = 7.6 Hz, 1H), 6.76 (d, *J* = 8.4 Hz, 1H), 4.32 (s, 1H), 3.88 (s, 3H), 3.24 (s, 3H), 3.12 (s, 3H); ¹³C NMR (100 MHz, CDCl₃) δ 171.96, 169.17, 155.42, 144.53, 137.59, 133.73, 132.01, 132.01, 129.39, 128.67, 128.41, 128.41, 128.37, 125.98, 121.63, 121.48, 113.48, 133.14, 107.84, 107.69, 56.21, 47.82, 45.69, 40.07, 27.05, 26.78; IR (neat) 2925, 2854, 1708, 1610, 1466 cm⁻¹; HRMS (ESI) *m/z* 445.1328 [C₂₆H₂₁ClN₂O₃ (M+H) requires 445.1313]; m.p. >220 °C.

3'-(4-Fluorophenyl)-1-methyldispiro[indoline-3,1'-cyclopropane-

2',3''-indoline]-2,2''-dione (4b). A solution of trifluoroacetic acid (57 mg, 0.5 mmol, 38 μL) in CH₂Cl₂ (0.2 mL) was added dropwise to a stirred solution of **10a** (18.6 mg, 0.04 mmol) in CH₂Cl₂ (0.10 mL) at rt and stirred for 3 h. The resulting solution was then diluted with CH₂Cl₂ (1 mL) and neutralized with saturated aqueous NaHCO₃ (2 mL), transferred to a

FULL PAPER

separatory funnel, and the layers separated. The aqueous phase was extracted with CH₂Cl₂ (3 x 3 mL) and the combined organic extracts were washed with saturated aqueous NaCl (4 mL) then concentrated under reduced pressure to provide 15 mg (quant.) of **4b** as a light yellow solid. ¹H NMR (500 MHz, CDCl₃) δ 8.24 (s, 1 H), 8.01 (d, *J* = 7.8 Hz, 1 H), 7.26-7.23 (m, 2 H), 7.11-7.7.08 (m, 2 H), 7.07-7.05 (m, 2 H), 6.97 (m, 2 H), 6.88 (td, *J* = 7.8, 1.2 Hz, 1 H), 6.83 (d, *J* = 7.8 Hz, 1 H), 6.80 (d, *J* = 7.8 Hz, 1 H), 4.36 (s, 1 H), 3.22 (s, 3 H); ¹³C NMR (150 MHz, CDCl₃) δ 171.6, 171.5, 163.0, 161.4, 144.3, 140.7, 132.1, 132.1, 128.9, 128.2, 128.2, 126.1, 125.3, 125.3, 125.1, 121.6, 121.2, 121.1, 115.0, 114.9, 109.1, 107.6, 48.0, 45.7, 39.6, 26.8; IR (neat) 3143, 3079, 3002, 1706, 1608, 1512, 1469, 1342, 1085, 833, 745 cm⁻¹; HRMS (ESI) *m/z* 385.1369 [C₂₄H₁₈FN₂O₂ (M+1) requires 385.1347]; *m.p.* > 220 °C.

3'-(4-Chlorophenyl)-1-methylspiro[indoline-3,1'-cyclopropane-2',3''-indoline]-2,2"-dione (4c). A solution of trifluoroacetic acid (35.1 mg, 0.31 mmol, 24 μL) in CH₂Cl₂ (0.12 mL) was added dropwise to a stirred solution of **10b** (11.2 mg, 0.02 mmol) in CH₂Cl₂ (0.10 mL) at rt and stirred for 3 h. The resulting solution was then diluted with CH₂Cl₂ (1 mL) and neutralized with saturated aqueous NaHCO₃ (2 mL), transferred to a separatory funnel, and the layers separated. The aqueous phase was extracted with CH₂Cl₂ (3 x 3 mL) and the combined organic extracts were washed with saturated aqueous NaCl (4 mL) then concentrated under reduced pressure to provide 9 mg (quant.) of **4c** as a white solid. ¹H NMR (500 MHz, CDCl₃) δ 8.17 (s, 1 H), 8.05 (d, *J* = 7.8 Hz, 1 H), 7.32-7.28 (m, 4 H), 7.15 (d, *J* = 7.5 Hz, 2 H), 7.07 (d, *J* = 7.5 Hz, 2 H), 6.94 (td, *J* = 7.65, 1.0 Hz, 1 H), 6.89-6.85 (comp, 2 H), 4.39 (s, 1 H), 3.26 (s, 3 H); ¹³C NMR (150 MHz, CDCl₃) δ 171.7, 171.6, 144.5, 140.9, 133.7, 132.0, 129.0, 128.4, 128.4, 128.4, 128.3, 126.2, 125.9, 125.2, 124.1, 121.8, 121.3, 121.3, 112.4, 109.3, 107.8, 48.0, 45.9, 39.7, 29.8, 27.0; IR (neat) 3245(b), 3084, 2924, 1707, 1612, 1492, 1469, 1339, 1087; HRMS (ESI) *m/z* 423.0886 [C₂₄H₁₇ClN₂O₂ (M+Na) requires 423.0871]; *m.p.* > 220 °C.

Cell culture. Human breast cancer cell lines MDA-MB-231 and MDA-MB-231-Br were cultured in DME/F12 with 10% fetal bovine serum (FBS), 2.5 mM L-Glutamine, 15 mM HEPES and penicillin (100 unit/mL)/streptomycin (100 μg/mL). All cell lines were maintained and grown in a 37 °C incubator with 5% CO₂. Parental MDA-MB-231 cells were purchased from ATCC. The MDA-MB-231-Br cell line was developed by *in vivo* selection of brain trophic sub-lines by a minimum of three rounds of intracardiac injection.

EC₅₀ determination. To generate a randomized plate for compound screening, all compounds were first solubilized in DMSO at 10 mM. 10 mM compounds were serially 1:10 diluted into DMSO to span a concentration range from 10 mM to 1 nM. An Eppendorf EpMotion 5075 robotic pipettor followed a randomization program to dilute compounds 1:10 into DME/F12 medium without FBS. The randomized plate contained compounds in 10% DMSO spanning a concentration range from 1 mM to 100 pM. Cells were plated in 96 well tissue culture plates at a concentration of 1,000 cells/well in 90 μL of medium, and given overnight to adhere. 10 μL of compound was pipetted from the randomized plates to the cell plates, yielding a working solution of 1% DMSO, with compound concentrations ranging from 100 μM to 10 pM. Plates were incubated for four days, then fixed and stained using a sulforhodamine B assay.²⁷ Briefly, medium was removed and cells were fixed in 10% trichloroacetic acid (Sigma-Aldrich) for one hour. Plates were rinsed repeatedly in deionized water and dried, prior to staining with a solution of 0.4% sulforhodamine B (Sigma-Aldrich) in 1% acetic acid (Sigma-Aldrich). Following one hour of staining, plates were rinsed 5 times in 1% acetic acid, and dried. 100 μL of 10 mM tris base was used to solubilize each well. Plates were incubated on an orbital shaker for 10-20 minutes to ensure full solubilization, and absorption at 554 nm was read on a BioTek Synergy H1 plate reader. Deconvolution of the randomization was performed in MATLAB (MathWorks), and EC₅₀ values were calculated by performing a non-linear four parameter curve fit in Prism 6 (GraphPad Software). Three technical replicates were performed for each experiment, and all experiments were repeated three times.

RNA-sequencing and molecular mechanism of action prediction.

MDA-231-Br cells were plated in 6 well plates such that they would be 70% confluent and allowed to adhere overnight. Cells were treated with **4b** at the five times the EC₅₀ value, 62.5 μM. Cells were collected in triplicate at 6, 12 and 24 hours post treatment, and RNA extracted with the PureLink kit (Invitrogen). Libraries for RNA sequencing were prepared according to the SmartSeq2 protocol.²⁸ Briefly, mRNA was specifically amplified using a primer complimentary to the polyA tail, and a template-switching oligonucleotide. This primer combination makes it possible to perform subsequent polymerase chain reaction (PCR) amplifications with a single primer set. Following first round amplification of whole mRNA sequences, a transposase-based system (Illumina Nextera XT DNA sample preparation kit) is used for fragmentation, where each library is broken into 300-800 bp fragments, which are tagged on both ends. This product is then PCR amplified using a bar-coded primer, so that multiple libraries can be pooled for a single sequencing run. All 12 sequencing libraries were run together in a single run on the Illumina MiSeq machine, using the V3 150 cycle kit, programmed for dual-end 75 bp reads. Following RNA sequencing, transcripts were aligned to the genome, and read counts were normalized using the TopHat and Cufflinks suite of tools.²⁹ DeMAND analysis was performed in R using the BioConductor software provided with the original manuscript.¹⁸ One modification was made to the RNA-sequencing data to facilitate the use of DeMAND. The DeMAND algorithm was developed for use on microarray data, which is significantly noisier than RNA-sequencing data due to the nature of the technology – reading fluorescence versus counting transcripts. Microarray data will never yield three identical values across biological replicates, while RNA-sequencing can yield identical replicates, particularly for undetectable transcripts, which will have zero counts across all replicates. To estimate the probability that the change in gene expression between vehicle and treatment is greater than would be expected randomly, DeMAND compares probability density functions. The probability density functions are generated by performed kernel density smoothing on the experimental replicates for each gene. Kernel density smoothing cannot be applied to three identical values; therefore, to facilitate the use of DeMAND to analyze our RNA-sequencing data we added noise to our data in the form of random values drawn from a normal distribution with mean = 0.1% of the maximum read count, and standard deviation = 0.01% of the maximum read count. We examined the robustness of the DeMAND algorithm to 0.01%, 0.1%, 1% and 10% noise, and verified that the addition of noise did not alter the results. For analysis of broad drug mechanism of action classes, multiple gene annotation sets were combined. Apoptosis: GO biological process – Regulation of apoptosis, GO biological process – Apoptotic program. Cell cycle: GO biological process – Regulation of the cell cycle, Biocarta – Cell cycle pathway. Ribosome: KEGG – Ribosome, GO biological process – Ribosome biogenesis and assembly. Microtubule disruption: GO biological processes – Microtubule polymerization or depolymerization, Reactome – Formation of tubulin folding intermediates, GO biological processes – Microtubule cytoskeleton organization and biogenesis. DNA damage: KEGG mismatch repair, KEGG non-homologous end joining, KEGG nucleotide excision repair. Kinase activation: GO biological processes – Activation of protein kinase activity, GO molecular function – Kinase regulator activity. GPCR activation: Biocarta – GPCR pathway, Reactome – Signaling by GPCR. Ion channel signaling: GO molecular function – Extracellular ligand gated ion channel activity, GO molecular function – Ion channel activity, GO molecular function – Ligand gated channel activity. For each gene in the combined gene set, the rank in the DeMAND. The genes predicted by DeMAND to be affected by **4b** treatment were ranked, with 1 being the gene whose regulon was most significantly altered by treatment. The rank of each gene in the combined gene sets was plotted.

Protein assay. MDA-231-Br cells were plated in 96 well tissue culture plates at a concentration of 10,000 cells/well in 90 μL of medium, and given overnight to adhere. Treatments were prepared in medium at 10x EC₂₅ concentrations and 10 μL was pipetted to the cell plates, yielding a working solution of 1% DMSO, with EC₂₅ concentrations – doxorubicin (1.14 μM), paclitaxel (0.05 μM), **4b** (62.3 μM). Cells were lysed in RIPA lysis buffer (ThermoFisher, 89900), with the addition of 2% SDS, and protease and

FULL PAPER

phosphatase inhibitor (Life Technologies, 88668) according to the manufacturer's instructions. Lysate was assayed for protein concentration using the Pierce BCA protein assay kit (ThermoFisher, 23225) according to the manufacturer's instructions.

Phalloidin staining. At the protein assay endpoint, cells were stained with Alexa Fluor 594 Phalloidin (ThermoFisher, A12381) according to the manufacturer's instructions. Briefly, cells were washed twice with PBS, fixed in 4% PFA for ten minutes, washed twice with PBS, and permeabilized with 0.1% Triton-X for 5 minutes. Cells were washed twice with PBS, blocked with 1% BSA in TBST for 5 minutes, and stained with phalloidin in 1% BSA in TBST for 20 minutes. Cells were counterstained with DAPI to show nuclei, washed twice with PBS and imaged in PBS. Imaging was performed on an EVOS FL system (Life Technologies) with a 20x objective.

Protein synthesis assay. MDA-231 cells were plated on cover slips at a concentration of 5,000 cells/slip in 90 μ L of medium, and given overnight to adhere. Treatments were prepared in medium at 5x EC₅₀ concentrations and 10 μ L was pipetted to the cell plates, yielding a working solution of 1% DMSO, with EC₅₀ concentrations – doxorubicin (2 μ M), paclitaxel (0.05 μ M), **4b** (100 μ M). After treatment, the drug-containing medium was removed and replaced with a solution of methionine-free media and Click-iT® HPG (an alkyne-containing methionine derivative). The cells were incubated for 30 minutes. Then, the Click-iT® HPG solution was removed, and the cells were washed once with PBS. Then the cells were fixed with 3.7% formaldehyde in PBS, incubated for 20 minutes, washed twice with 3% BSA in PBS, permeabilized with 0.5% Triton in PBS, and incubated for 20 minutes. Newly synthesized protein was detected using the Click-iT™ HPG Alexa Fluor™ 488 Protein Synthesis Assay Kit (ThermoFisher C10428) according to the manufacturer's instructions.

Protein detection. At the protein assay endpoint, the permeabilization solution was removed, and cells were washed twice with 3% BSA in PBS. Click-iT® reaction cocktail (prepared according to the manufacturer's instructions) was added to each coverslip, and the cells were allowed to incubate for 30 minutes, protected from light. The reaction cocktail was removed, and the cells were washed once with Click-iT® reaction rinse buffer. Cell DNA was stained with HCS NuclearMask™ Blue Stain, and the cells were allowed to incubate for 30 minutes, protected from light. The staining solution was removed, and the cells were washed twice with PBS. Imaging with performed on an EVOS FL system (Life Technologies) with a 20x objective.

Acknowledgements

This work was supported by a Walther Cancer Foundation Advancing Basic Cancer Research Program grant and the National Science Foundation (CAREER CHE-1056242 and CHE-1665440). E.P.B was supported by a K.X.R. was supported by a Walther Cancer Foundation ENSCCII Training Grant. E.N.H was supported by Indiana Clinical and Translational Sciences Institute Training Grant TL1R001107, and 1F32CA210583. M.B. was supported an American Cancer Society Institutional Research Grant IRG-14-195-01. We thank the Mike and Josie Harper Cancer Research Institute for their support.

Keywords: spirooxindoles • transcriptome network • drug discovery • natural products • mechanism of action

References:

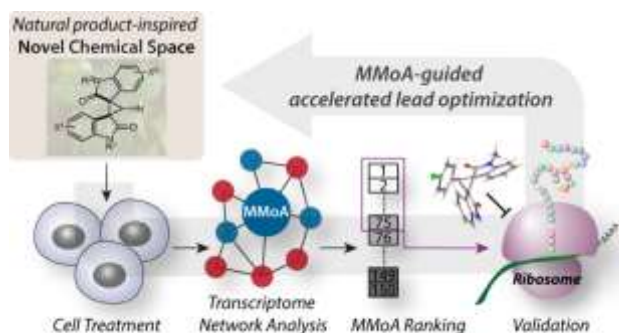
- [1] (a) Heath, J. R.; Ribas, A.; Mischel, P. S. *Nat. Rev. Drug Discovery* **2016**, *15*, 204-216. (b) Swinney, D. C.; Anthony, J. *Nat. Rev. Drug Discovery* **2011**, *10*, 507-519.
- [2] (a) Scannell, J. W.; Blanckley, A.; Boldon, H.; Warrington, B. *Nat. Rev. Drug Discovery* **2012**, *11*, 191-200. (b) Kotz, J. *SciBX* **2012**, *5*, 1-3.
- [3] (a) Harvey, A. L.; Edrada-Ebel, R.; Quinn, R. J. *Nat. Rev. Drug Discovery* **2015**, *14*, 111-129. (b) Wehling, M. *Nat. Rev. Drug Discovery* **2009**, *8*, 541-546. (c) Sukuru, S. C. K.; Jenkins, J. L.; Beckwith, R. E. J.; Scheiber, J.; Bender, A.; Mikhailov, D.; Davies, J. W.; Glick, M. *J. Biomol. Screen.* **2009**, *14*, 690-699.
- [4] (a) Wetzel, S.; Bon, R. S.; Kumar, K.; Waldmann, H. *Angew. Chem., Int. Ed.* **2011**, *50*, 10800-10826. (b) Yildirim, M. A.; Goh, K.-I.; Cusick, M. E.; Barabási, A.-L.; Vidal, M. *Nat. Biotechnol.* **2007**, *25*, 1119-1126.
- [5] (a) Kellenberger, E.; Hofmann, A.; Quinn, R. J. *Nat. Prod. Rep.* **2011**, *28*, 1483-1492. (b) Hert, J.; Irwin, J. J.; Laggner, C.; Keiser, M. J.; Shoichet, B. K. *Nat. Chem. Biol.* **2009**, *5*, 479-483. (c) Quinn, R. J.; Carroll, A. R.; Pham, N. B.; Baron, P.; Palframan, M. E.; Suraweera, L.; Pierens, G. K.; Muresan, S. *J. Nat. Prod.* **2008**, *71*, 464-468. (d) McArdle, B. M.; Campitelli, M. R.; Quinn, R. J. *J. Nat. Prod.* **2006**, *69*, 14-17. (e) Wess, G.; Urmann, M.; Sickenberger, B. *Angew. Chem., Int. Ed.* **2001**, *40*, 3341-3350. (f) Debouck, C.; Metcalf, B. *Annu. Rev. Pharmacol. Toxicol.* **2000**, *40*, 193-207.
- [6] Dai, Y.-F.; Zhao, X.-M. *Biomed Res Int* **2015**, *3*, 1-9.
- [7] (a) Imamura, S. *Cell Mol. Neurobiol.* **2013**, *33*, 129-135. (b) Yu, B.; Yu, D.-Q.; Liu, H.-M. *Eur. J. Med. Chem.* **2015**, *97*, 673-698.
- [8] (a) Antonchick, A. P.; Gerding-Reimers, C.; Catarinella, M.; Schürmann, M.; Preut, H.; Ziegler, S.; Rauh, D.; Waldmann, H. *Nat. Chem.* **2010**, *2*, 735-740. (b) Galliford, C. V.; Scheidt, K. A. *Angew. Chem., Int. Ed.* **2007**, *46*, 8748-8758. (c) Marti, C.; Carreira, Erick M. *Eur. J. Org. Chem.* **2003**, 2003, 2209-2219. (d) Monteiro, Â.; Gonçalves, L. M.; Santos, M. M. M. *Eur. J. Med. Chem.* **2014**, *79*, 266-272. (e) Rajesh, S. M.; Perumal, S.; Menéndez, J. C.; Yogeeswari, P.; Sriram, D. *MedChemComm* **2011**, *2*, 626-630. (f) Schönhaber, J.; Müller, T. J. J. *Org. Biomol. Chem.* **2011**, *9*, 6196-6199. (g) Yeung, B. K. S.; Zou, B.; Rottmann, M.; Lakshminarayana, S. B.; Ang, S. H.; Leong, S. Y.; Tan, J.; Wong, J.; Keller-Maerki, S.; Fischli, C.; Goh, A.; Schmitt, E. K.; Krastel, P.; Francotte, E.; Kuhen, K.; Plouffe, D.; Henson, K.; Wagner, T.; Winzeler, E. A.; Petersen, F.; Brun, R.; Dartois, V.; Diagana, T. T.; Keller, T. H. *J. Med. Chem.* **2010**, *53*, 5155-5164.
- [9] (a) Ball-Jones, N. R.; Badillo, J. J.; Franz, A. K. *Org. Biomol. Chem.* **2012**, *10*, 5165-5181. (b) Cheng, D.; Ishihara, Y.; Tan, B.; Barbas, C. F. *ACS Catalysis* **2014**, *4*, 743-762. (c) Xia, M.; Ma, R.-Z. *J. Heterocycl. Chem.* **2014**, *51*, 539-554.
- [10] Pavlovska, T. L.; Redkin, R. G.; Lipson, V. V.; Atamanuk, D. V. *Mol. Divers.* **2016**, *20*, 299-344.
- [11] (a) Jiang, T.; Kuhen, K. L.; Wolff, K.; Yin, H.; Bieza, K.; Caldwell, J.; Bursulaya, B.; Tuntland, T.; Zhang, K.; Karanewsky, D.; He, Y. *Bioorg. Med. Chem. Lett.* **2006**, *16*, 2109-2112. (b) Jiang, T.; Kuhen, K. L.; Wolff, K.; Yin, H.; Bieza, K.; Caldwell, J.; Bursulaya, B.; Wu, T. Y.-H.; He, Y. *Bioorg. Med. Chem. Lett.* **2006**, *16*, 2105-2108. (c) Sampson, P. B.; Liu, Y.; Patel, N. K.; Feher, M.; Forrest, B.; Li, S.-W.; Edwards, L.; Laufer, R.; Lang, Y.; Ban, F.; Awrey, D. E.; Mao, G.; Plotnikova, O.; Leung, G.; Hodgson, R.; Mason, J.; Wei, X.; Kiarash, R.; Green, E.; Qiu, W.; Chirgadze, N. Y.; Mak, T. W.; Pan, G.; Pauls, H. W. *J. Med. Chem.* **2015**, *58*, 130-146. (d) Stevens, F. C.; Bloomquist, W. E.; Borel, A. G.; Cohen, M. L.; Droste, C. A.; Heiman, M. L.; Kriauciunas, A.; Sall, D. J.; Tinsley, F. C.; Jesudason, C. D. *Bioorg. Med. Chem. Lett.* **2007**, *17*, 6270-6273. (e) Ye, N.; Chen, H.; Wold, E. A.; Shi, P.-Y.; Zhou, J. *ACS Infect. Dis.* **2016**, *2*, 382-392.
- [12] Reddy, C. N.; Nayak, V. L.; Mani, G. S.; Kapure, J. S.; Adiyala, P. R.; Maurya, R. A.; Kamal, A. *Bioorg. Med. Chem. Lett.* **2015**, *25*, 4580-4586.
- [13] (a) Wilson, E. E.; Rodriguez, K. X.; Ashfeld, B. L. *Tetrahedron* **2015**, *71*, 5765-5775. (b) Zhou, R.; Yang, C.; Liu, Y.; Li, R.; He, Z. *The Journal of Organic Chemistry* **2014**, *79*, 10709-10715.
- [14] Lipinski, C. A. *Drug Discov. Today Technol.* **2004**, *1*, 337-341.
- [15] Hewage, H. S.; Anslyn, E. V. *J. Am. Chem. Soc.* **2009**, *131*, 13099-13106.
- [16] Pajouhesh, H.; Lenz, G. R. *NeuroRx* **2005**, *2*, 541-553.
- [17] Hitchcock, S. A. *Curr. Opin. Chem. Biol.* **2008**, *12*, 318-323.

FULL PAPER

- [18] Woo, J. H.; Shimoni, Y.; Yang, W. S.; Subramaniam, P.; Iyer, A.; Nicoletti, P.; Rodríguez Martínez, M.; López, G.; Mattioli, M.; Realubit, R.; Karan, C.; Stockwell, B. R.; Bansal, M.; Califano, A. *Cell* **2015**, *162*, 441-451.
- [19] Szklarczyk, D.; Franceschini, A.; Wyder, S.; Forslund, K.; Heller, D.; Huerta-Cepas, J.; Simonovic, M.; Roth, A.; Santos, A.; Tsafou, K. P.; Kuhn, M.; Bork, P.; Jensen, L. J.; von Mering, C. *Nucleic Acids Res.* **2015**, *43*, D447-D452.
- [20] Subramanian, A.; Tamayo, P.; Mootha, V. K.; Mukherjee, S.; Ebert, B. L.; Gillette, M. A.; Paulovich, A.; Pomeroy, S. L.; Golub, T. R.; Lander, E. S.; Mesirov, J. P. *Proc. Natl. Acad. Sci. U.S.A.* **2005**, *102*, 15545-15550.
- [21] Hess, S. T.; Girirajan, T. P. K.; Mason, M. D. *Biophys. J.* **2006**, *91*, 4258-4272.
- [22] (a) Hoelder, S.; Clarke, P. A.; Workman, P. *Mol. Oncol.* **2012**, *6*, 155-176. (b) Moffat, J. G.; Rudolph, J.; Bailey, D. *Nat. Rev. Drug Discovery* **2014**, *13*, 588-602.
- [23] Bhat, M.; Robichaud, N.; Hulea, L.; Sonenberg, N.; Pelletier, J.; Topisirovic, I. *Nat. Rev. Drug Discovery* **2015**, *14*, 261-278.
- [24] (a) Ivashkin, P.; Couve-Bonnaire, S.; Jubault, P.; Pannecoucke, X. *Org. Lett.* **2012**, *14*, 2270-2273. (b) Li, C.; Guo, F.; Xu, K.; Zhang, S.; Hu, Y.; Zha, Z.; Wang, Z. *Org. Lett.* **2014**, *16*, 3192-3195.
- [25] (a) Li, J.; Wang, N.; Li, C.; Jia, X. *Chem. Eur. J.* **2012**, *18*, 9645-9650. (b) Wille, G.; Steglich, W. *Synthesis-Stuttgart* **2001**, 759-762. (c) Jie, H. H.; Li, J.; Li, C. J.; Jia, X. S. *Synlett* **2012**, *23*, 2274-2278.
- [26] Beauchard, A.; Ferandin, Y.; Frère, S.; Lozach, O.; Blairvacq, M.; Meijer, L.; Thiéry, V.; Besson, T. *Biorg. Med. Chem.* **2006**, *14*, 6434-6443.
- [27] (a) Voigt, W. *Sulforhodamine B assay and chemosensitivity*, 2005; Vol. 110. (b) Vichai, V.; Kirtikara, K. *Nat Protoc* **2006**, *1*, 1112-1116.
- [28] Picelli, S.; Faridani, O. R.; Bjorklund, A. K.; Winberg, G.; Sagasser, S.; Sandberg, R. *Nat Protoc* **2014**, *9*, 171-181.
- [29] (a) Trapnell, C.; Roberts, A.; Goff, L.; Pertea, G.; Kim, D.; Kelley, D. R.; Pimentel, H.; Salzberg, S. L.; Rinn, J. L.; Pachter, L. *Nat Protoc* **2012**, *7*, 562-578. (b) Trapnell, C.; Hendrickson, D. G.; Sauvageau, M.; Goff, L.; Rinn, J. L.; Pachter, L. *Nat. Biotechnol.* **2013**, *31*, 46-53.

FULL PAPER

Entry for the Table of Contents



This study demonstrates the value of an integrated, biologically-inspired synthesis and assay strategy for the identification of potential small molecule drug candidates. The combination of scaffold-directed synthesis in conjunction with a hybrid experimental/transcriptome analysis successfully identified a subset of bis-spirooxindole cyclopropanes that were shown to inhibit cancer cell proliferation through the disruption of ribosomal function.